Journal of Zhejiang University-SCIENCE B (Biomedicine & Biotechnology)
ISSN 1673-1581 (Print); ISSN 1862-1783 (Online)
www.jzus.zju.edu.cn; www.springerlink.com
E-mail: jzus@zju.edu.cn

Simulation of inter atrial block based on a human atrial model*

Yuan GAO[§1], Ying-lan GONG[§1], Ling XIA[†‡1], Ding-chang ZHENG[2]

[1]*Key Laboratory for Biomedical Engineering of Ministry of Education, Department of Biomedical Engineering, Zhejiang University, Hangzhou 310027, China*

[2]*Health and Wellbeing Academy, Faculty of Medical Science, Anglia Ruskin University, Chelmsford, CM1 1SQ, UK*

[†]E-mail: xialing@zju.edu.cn

Received Aug. 7, 2018; Revision accepted Oct. 29, 2018; Crosschecked Mar. 2, 2019

Abstract: Inter atrial block (IAB) is a prevailing cardiac conduction abnormality that is under-recognized in clinical practice. IAB has strong association with atrial arrhythmia, left atrial enlargement, and electromechanical discordance, increasing the risk of atrial fibrillation (AF) and myocardial ischemia. IAB was generally believed to be caused by impaired conduction along the Bachmann bundle (BB). However, there are three other conduction pathways, including the fibers posteriorly in the vicinity of the right pulmonary veins (VRPV), transseptal fibers in the fossa ovalis (FO), and muscular bundles on the inferior atrial surface near the coronary sinus (CS). We hypothesized that the importance of BB on IAB might have been overestimated. To test this hypothesis, various combinations of conduction pathway blocks were simulated based on a realistic human atrial model to investigate their effects on the index of clinical diagnosis standard of IAB using a simulated 12-lead electrocardiogram (ECG). Firstly, the results showed that the BB block alone could not generate typical P wave morphology of IAB, and that the combination of BB and VRPV pathway block played important roles in the occurrence of IAB. Secondly, although single FO and CS pathways play subordinate roles in inter atrial conduction, their combination with BB and VRPV block could also produce severe IAB. In summary, this simulation study has demonstrated that the combinations of different inter atrial conduction pathways, rather than BB alone, resulted in ECG morphology of IAB. Attention needs to be paid to this in future pathophysiological and clinical studies of IAB.

Key words: Inter atrial block; Electrocardiogram; Simulation; Heart model
https://doi.org/10.1631/jzus.B1800420 **CLC number:** R540.4

1 Introduction

Inter atrial block (IAB) is defined as a prolonged conduction time between the right and left atriums due to impulse delay or blockage, leading to prolonged P wave duration (>120 ms) on a surface electrocardiogram (ECG) (Tse et al., 2017). IAB can be graded as partial and advanced, depending on the severity of the conduction delay (Kitkungvan and Spodick, 2009; Bayés de Luna et al., 2012). Partial IAB is characterized by bifid morphology of ECG P waves on leads I, II, III, and aVF. While advanced IAB is characterized by biphasic P waves on lead V_1 and inferior leads (II, III, and aVF) (Tse et al., 2016; Martínez-Sellés et al., 2017). IAB was first described experimentally by Bachmann (1916). Unlike other common cardiac diseases, IAB is still poorly perceived and is underappreciated in clinical practice, despite its high prevalence in inpatient and outpatient populations (Spodick and Ariyarajah, 2009; Chhabra et al., 2014).

The prevalence of IAB is age-dependent, increasing from about 5% for individuals under 20 years old to 60% at ages over 50 years (Gialafos et al., 2007; Martínez-Sellés et al., 2016). IAB can lead to delayed and asynchronous activation of the left atrium, increasing the risks of atrial arrhythmias and ischemic

‡ Corresponding author
§ The two authors contributed equally to this work
* Project supported by the National R&D Program for Major Research Instruments of China (No. 61527811), the National Natural Science Foundation of China (No. 61701435), and the Zhejiang Provincial Natural Science Foundation of China (No. LY17H180003)
ORCID: Ling XIA, https://orcid.org/0000-0002-1937-9693

stroke (Ariyarajah et al., 2007a; He et al., 2017), left atrial (LA) enlargement, LA electromechanical dysfunction, and thromboembolism (Wu et al., 2017). Previous studies have suggested that IAB is a potential risk factor of atrial fibrillation (AF) (Bayés de Luna et al., 2017; Massó-van Roessel et al., 2017). The presence of IAB was shown to be related to the development of new onset and recurrence of AF (Enriquez et al., 2015; Alexander et al., 2017; Fernández-Fernández, 2017; Tekkesin et al., 2017). Moreover, IAB is associated with the deterioration of paroxysmal AF into chronic and permanent forms (Abe et al., 1997).

However, the underlying mechanism directly affecting IAB has not been fully elucidated. Coronary artery disease and other common cardiovascular risk factors, such as diabetes mellitus, hypertension, hypercholesterolemia, obesity, smoking, and physical inactivity, have been proposed to be the pathogenesis of IAB (Ariyarajah and Spodick, 2006; Ariyarajah et al., 2007b). IAB is generally considered to be caused by impaired conduction along the Bachmann bundle (BB) (O'Neal et al., 2016; Tse et al., 2016). However, there are three other conduction pathways, including the fibers posteriorly in the vicinity of the right pulmonary veins (VRPV), transseptal fibers in the fossa ovalis (FO), and muscular bundles on the inferior atrial surface near the coronary sinus (CS). Tapanainen et al. (2009) studied the conduction pathway in patients with paroxysmal AF, and concluded that BB might not exclusively serve as the preferential or dominant route for inter atrial conduction. This implies that the importance of BB in IAB may be overestimated.

The main aim of this study was to investigate the combined effect of the four inter atrial pathway blocks on the occurrence of IAB. To achieve this, various combinations of conduction pathway blocks would be simulated based on a realistic human atrial model, and the simulated 12-lead ECG would be used to test their effect on the index of the standard clinical diagnosis of IAB.

2 Materials and methods

2.1 Anatomical model

The atrial model was constructed based on a healthy adult male heart specimen obtained from Zhujiang Hospital, Southern Medical University, Guangzhou, China. The Chinese Law on Heart Research using a heart specimen has been strictly followed. The specimen was scanned using spiral computerized tomography (Philips/Brilliance 64, the Netherlands) with a resolution of 512 pixels×512 pixels and the spatial resolution was 0.3574 mm×0.3574 mm×0.3300 mm (Fig. 1). Details of the model can be found in our previous study (Deng et al., 2012a, 2012b; Gong et al., 2015).

The conduction system in the constructed model consisted of a sinus node (SAN), crista terminalis (CT), pectinate muscle (PM), and inter atrial impulse propagation routes. The inter atrial conduction pathways included BB, VRPV, FO, and CS. The atrial fiber orientation was contained to simulate the anisotropy. The atrial cell in this study was based on the model developed by Courtemanche et al. (1998). During the activation propagation, each myocardial unit has specific electrophysiological parameters associated with the action potential (AP) of the cell unit and conduction velocity.

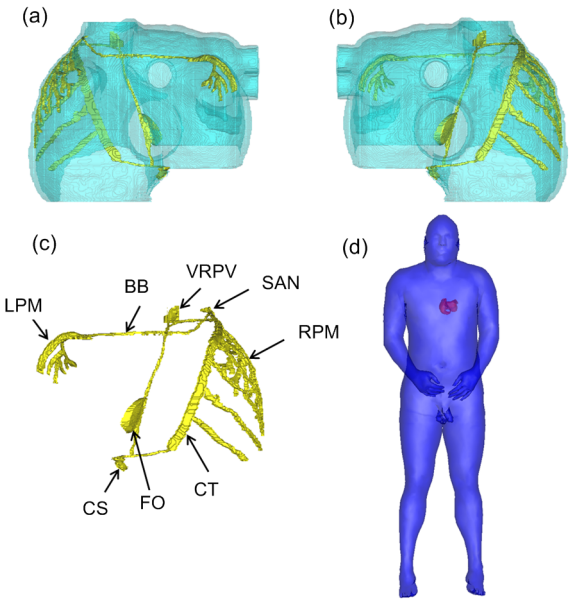

Fig. 1 Illustration of the atrium and torso model
(a) Anterior view of atrium; (b) Posterior view of atrium. The cyan color indicates atrial muscles, and the yellow color indicates the conduction system. (c) Conduction system; (d) Merge of the atrium into the body. LPM: left atrium pectinate muscle; BB: Bachmann bundle; VRPV: vicinity of the right pulmonary veins; SAN: sinus node; RPM: right atrium pectinate muscle; CT: crista terminalis; FO: fossa ovalis; CS: coronary sinus (Note: for interpretation of the references to color in this figure legend, the reader is referred to the web version of this article)

2.2 Numerical method

The excitation conduction was simulated based on the monodomain equation (Zhang et al., 2007):

$$\frac{\partial V_{\mathrm{m}}}{\partial t}=\frac{1}{C_{\mathrm{m}}}\left(\frac{1}{A_{\mathrm{m}}}\left(\frac{\lambda}{1+\lambda}\nabla\cdot\left(\sigma_{\mathrm{i}}\nabla V_{\mathrm{m}}\right)-I_{\mathrm{ion}}+I_{\mathrm{app}}\right)\right), \quad (1)$$

where V_{m} is the transmembrane voltage, t is time, C_{m} is the membrane capacitance, A_{m} is the surface to volume ratio, λ is the ratio of conductivity extracellular to intracellular, σ_{i} is the cellular conductivity, I_{ion} is the sum of ionic currents, and I_{app} is the sum of applied stimulus currents.

Eq. (1) was solved numerically using the explicit Euler method based on parallel computational techniques. The simulation was computed on a cluster of networked Dawning TC4000L systems (Sugon, China). It had multiple symmetrical parallel processors that contained a management node and ten computation nodes. Each computation node consisted of two Intel Xeon 5335 processors (each 4-core) and 4 GB memory. The total theoretical computing capacity was up to 184 Gflops (giga floating-point operations per second). MPICH2 was used to implement the communication between nodes.

In this study, the torso model was taken from a virtual male subject of the United States (Ackerman, 1991). The body surface potentials generated by the cardiac sources satisfy the Poisson equation with Newman boundary conditions:

$$\begin{cases}\nabla\cdot(\sigma\nabla\Phi)=-\nabla\cdot\boldsymbol{J}_{\mathrm{s}}, & \text{in } \Omega,\\ \sigma(\nabla\Phi)\cdot\boldsymbol{n}=0, & \text{on } S_{\mathrm{B}},\end{cases} \quad (2)$$

where σ is a tissue-dependent conductivity tensor, Φ is the quasi static potential, $\boldsymbol{J}_{\mathrm{s}}$ is the density of the equivalent dipole sources, $\boldsymbol{n}$ is the normal vector, and S_{B} is the body surface which encloses the volume conductor Ω.

Using the Green second identity:

$$\int_S(A\nabla B-B\nabla A)\cdot\boldsymbol{n}\,\mathrm{d}S=\int_V(A\nabla^2B-B\nabla^2A)\,\mathrm{d}\Omega, \quad (3)$$

where $A=1/R$ ($R=|\boldsymbol{r}-\boldsymbol{r}_{\mathrm{s}}|$ is the distance between the field point $\boldsymbol{r}$ and source point $\boldsymbol{r}_{\mathrm{s}}$) and $B=\sigma\Phi$, S is the boundary surface, and V is the volume, the differential equation for Φ as Eq. (2) can be solved as follows:

$$\Phi(\boldsymbol{r})=\frac{1}{4\pi\sigma}\left(\int_{\Omega_{\mathrm{h}}}\boldsymbol{J}_{\mathrm{s}}\cdot\nabla\frac{1}{R}\mathrm{d}V+\sum_{l=1}^{m}\left(\sigma_l^{+}-\sigma_l^{-}\right)\int_{S_l}\Phi(\boldsymbol{r})\nabla\frac{1}{R}\mathrm{d}S\right), \quad (4)$$

where Ω_{h} is the heart area, S_l (l=1, 2, …, m) is the conductivity junction surface, and its inside and outside conductivities are σ_l^{-} and σ_l^{+}, respectively. Further details of the model were described in our previous studies (Xia et al., 2006; Shou et al., 2007; Gao et al., 2018).

The 12-lead ECGs are calculated as described by Kligfield et al. (2007):

$$\begin{aligned}&\mathrm{I}=V_{\mathrm{LA}}-V_{\mathrm{RA}},\ \mathrm{II}=V_{\mathrm{LL}}-V_{\mathrm{RA}},\ \mathrm{III}=V_{\mathrm{LL}}-V_{\mathrm{LA}},\\&\mathrm{aVR}=-1/2(\mathrm{I}+\mathrm{II}),\ \mathrm{aVL}=\mathrm{I}-1/2\mathrm{II},\ \mathrm{aVF}=\mathrm{II}-1/2\mathrm{I},\\&\mathrm{V}_i=V_{\mathrm{P}i}-(V_{\mathrm{LA}}+V_{\mathrm{RA}}+V_{\mathrm{LL}})/3,\end{aligned} \quad (5)$$

where V_{LA} is left arm surface potential, V_{RA} is right arm surface potential, V_{LL} is left leg surface potential, V_i is each precordial lead (i=1, 2, …, 6), and $V_{\mathrm{P}i}$ is each precordial surface potential.

3 Results

3.1 One conduction pathway block alone

Fig. 2 shows the exciting sequence maps of atrium with one conduction pathway block alone. For comparison, the normal atrial exciting sequence maps are also presented at the top of Fig. 2. The normal depolarization duration of the right atrium was 86 ms. The initial onset of LA activation through the BB conduction pathway was located at the anterior wall near the LA appendage at 37 ms. The total depolarization time of the atrium was 103 ms at the area of the posterior LA wall.

With the conduction pathway block of BB only, the activation wave has to pass through the other three pathways from the atrial septum. This extended the propagation distance and prolonged the total depolarization time of the atrium to 113 ms.

With the conduction pathway block of VRPV only, since the BB pathway was in a normal condition, the exciting sequence of the LA anterior wall had no obvious change, but the activation wave from the right atrial (RA) posterior wall to the LA posterior wall was apparently separated. The activation wave had to pass through the BB and propagated across the roof of the LA to converge with the wave that passed

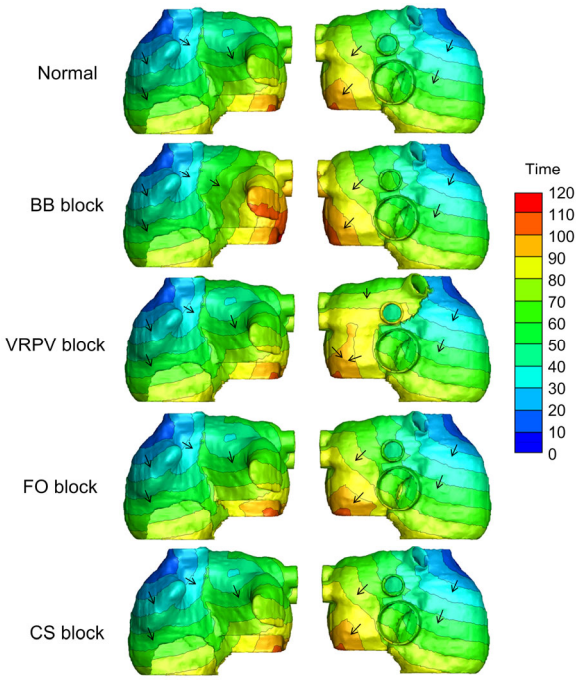

Fig. 2 Simulated activation sequences with one conduction pathway block alone

The arrows indicate the wave propagation direction. The color bar on the right-hand side indicates the propagation time with the unit in milliseconds (Note: for interpretation of the references to color in this figure legend, the reader is referred to the web version of this article)

through the FO pathway. This changed the exciting sequence of the LA posterior wall, but the propagation direction was still forward and the total depolarization time was only prolonged to 104 ms.

With the conduction pathway block of FO only, the activation wave passed through the VRPV pathway and propagated to the area that should have been activated by the FO pathway, so the atrial exciting sequence maps were similar to the normal case. The total depolarization time of the atrium was 105 ms. Finally, with the block of SC only, the activation wave could pass through FO and propagated to the area that should have been activated by the CS pathway, so the atrial exciting sequence maps had no change in comparison with the normal case and the total depolarization time of the atrium was also 103 ms.

Figs. 3 and 4 show the P wave of the simulated 12-lead ECG of atrium with one conduction block in comparison with a normal atrium. When the BB conduction pathway alone was blocked, the atrial total depolarization time was obviously prolonged, leading the ECG P wave duration up to 113 ms, but this did not reach the IAB criterion (P wave duration >120 ms). Likewise, the morphology of the P wave was still positive. This is because the VRPV conduction pathway was in a normal condition, so the

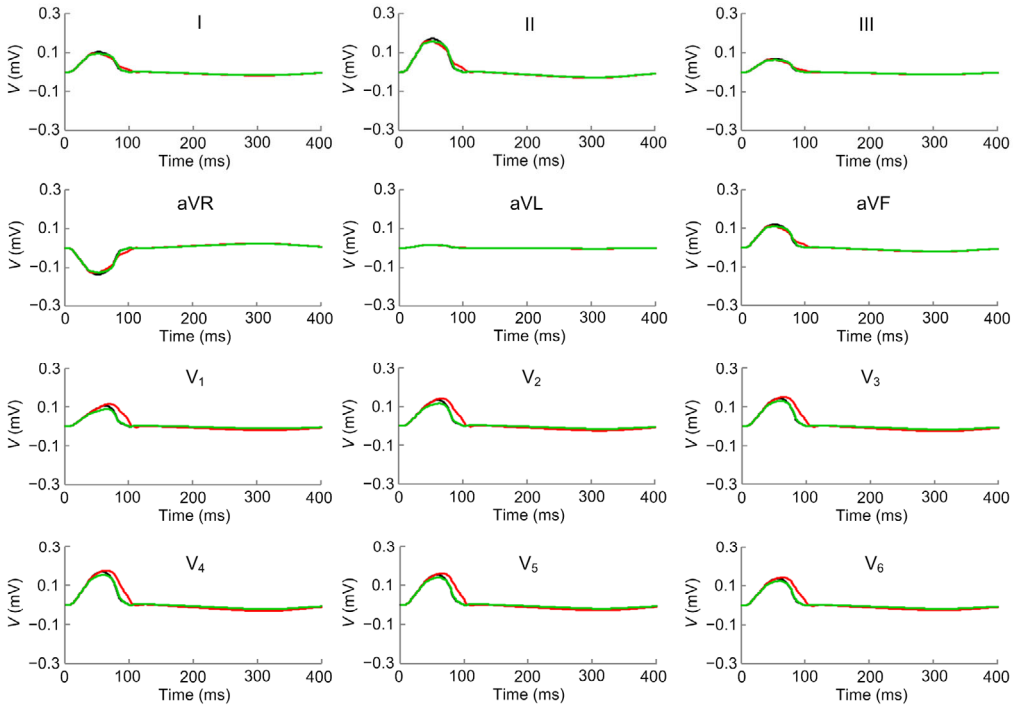

Fig. 3 Simulated P waves of 12-lead ECG with one conduction pathway (BB or VRPV) block alone

The black lines are from the normal cases, red lines are with BB block and green lines with VRPV block (Note: for interpretation of the references to color in this figure legend, the reader is referred to the web version of this article)

activation wave still could propagate from the superior of the LA.

When the VRPV conduction pathway was blocked alone, the exciting sequence of the atrial posterior wall was changed, but the propagation direction was still forward, with the result that there was no obvious difference in the P wave in comparison with the normal case. As shown in Fig. 4, when the FO or CS conduction pathway was blocked alone, the atrial exciting sequence barely changed, and the P wave was nearly the same as the normal case.

3.2 Block of two conduction pathways

Fig. 5 shows exciting sequence maps of the atrium with the block from two conduction pathways. When the two superior pathways (BB and VRPV) were both blocked, the activation wave could only pass through inferior pathways (FO and CS). This led to the retrograde activation of LA in the caudo-cranial direction. The total depolarization time of atrium was prolonged to 124 ms. With the block of BB+FO or BB+CS, the activation wave could pass through the normal VRPV and the wave still propagated in a forward direction. The total depolarization time of the atrium was 114 and 113 ms, respectively.

Fig. 6 shows the simulated P wave of the 12-lead ECG of the atrium with two conduction blocks. When the BB and VRPV conduction pathways were blocked, the retrograde activation of LA resulted in biphasic P waves in lead V_1 and the inferior leads (II, III, and aVF), leading to a prolonged P wave duration of 124 ms. Both the P wave morphology and duration time satisfied the diagnostic criteria of IAB. When the conduction pathways of BB+FO or BB+CS were blocked, the simulated morphology of the P wave was still positive.

3.3 Block of three conduction pathways

Fig. 7 shows the exciting sequence maps of atrium with the block of three conduction pathways. When the BB, VRPV, and FO were blocked, the activation wave had to propagate to the CS pathway first, and then retrograded to LA, leading to propagation distance and resulting in the significantly prolonged depolarization time of the atrium of 160 ms. Similarly, with the block of BB, VRPV, and CS, the activation

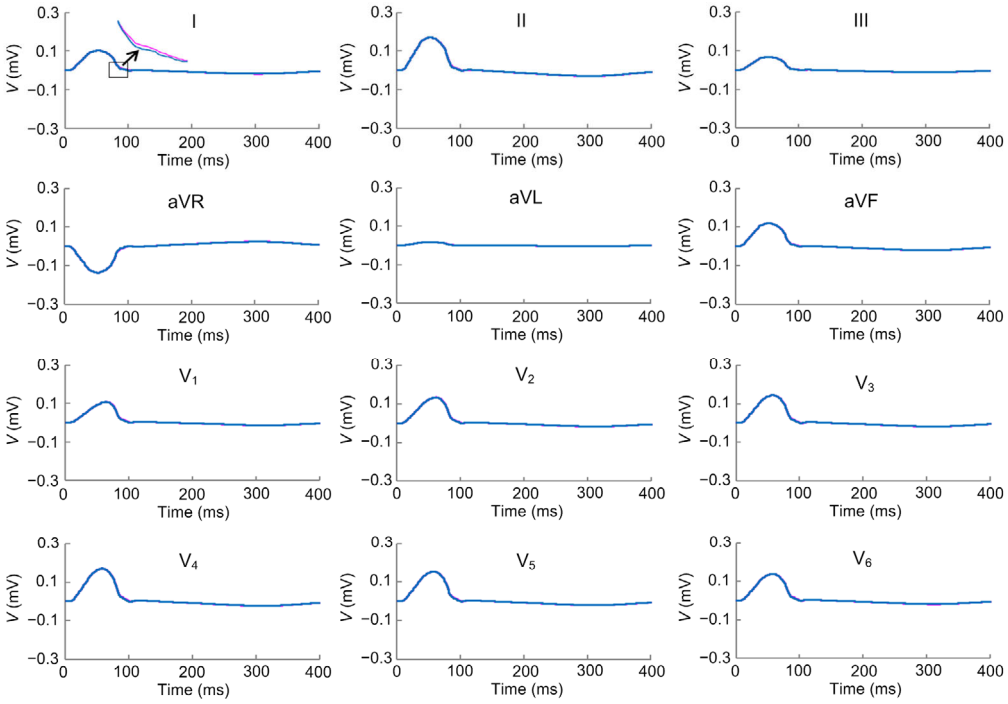

Fig. 4 Simulated P waves of 12-lead ECG with one conduction pathway (FO or CS) block alone

The black lines are the normal cases, pink lines are with FO block and blue lines with CS block. As the FO and CS blocks were similar to normal case, the lines were overlapped. On lead I, a local enlarged window is given to illustrate the minor differences (Note: for interpretation of the references to color in this figure legend, the reader is referred to the web version of this article)

wave had to pass through the FO pathway first, and then retrograded to LA. While the propagation speed at FO is superior to the CS pathway, the depolarization time of atrium was prolonged to 124 ms.

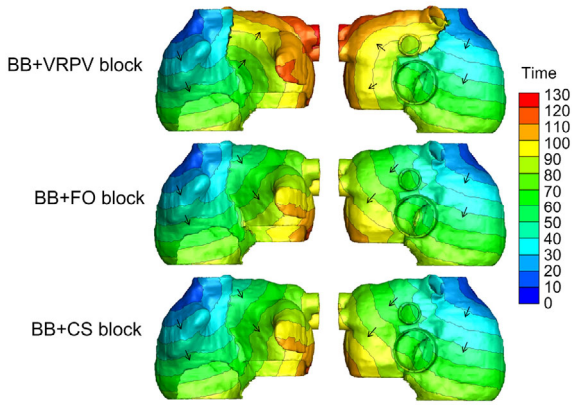

Fig. 5 Simulated activation sequences with the block of two conduction pathways

The arrows indicate the wave propagation direction. The color bar on the right-hand side indicates the propagation time with the unit in milliseconds (Note: for interpretation of the references to color in this figure legend, the reader is referred to the web version of this article)

Fig. 8 shows the simulated P wave of the 12-lead ECG of atrium with the block of three conduction pathways. The blocks of BB+VRPV+FO and BB+VRPV+CS both produced significant biphasic P waves in lead V_1 and the inferior leads.

Table 1 gives a summary of P wave duration and morphology with different combinations of conduction pathway blocks. It can be seen that, to achieve the criteria of IAB, the combinational block of BB and VRPV was required.

4 Discussion

This study investigated the effects of IAB with various conduction pathway block combinations. The simulation results indicated that the block of BB could only increase the P wave duration by 10 ms, but the morphology and polarity remained normal. With the block of the other three conduction pathways (VRPV, FO, or CS), no obvious change in P wave duration or morphology was observed. The simulation results were in accordance with reported data from canine

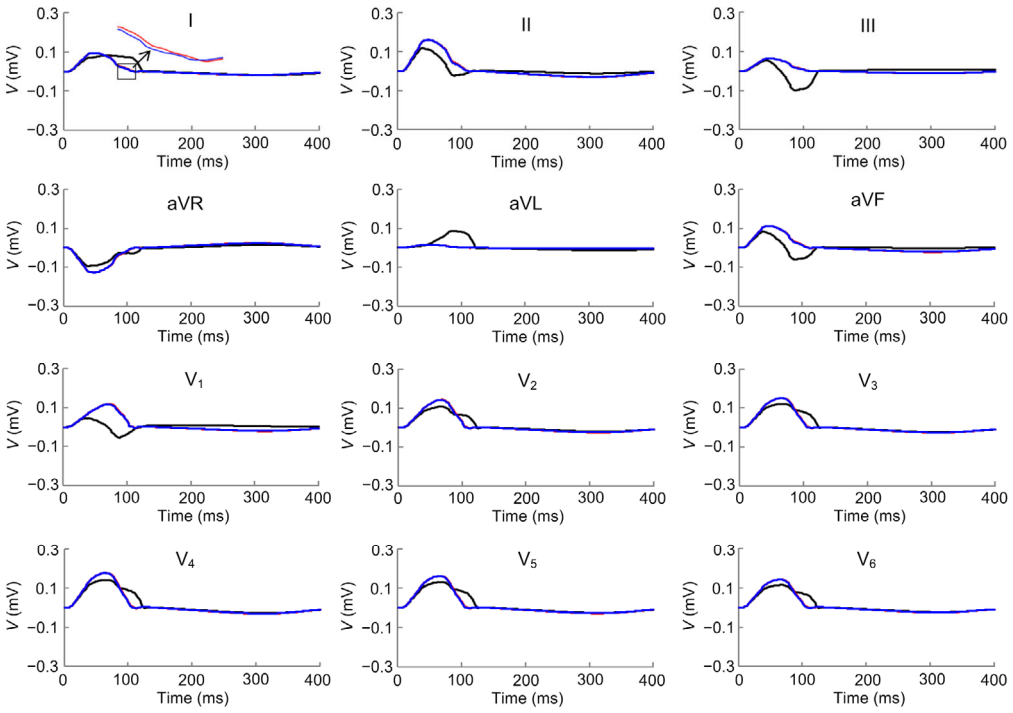

Fig. 6 Simulated P waves of 12-lead ECG with the block of two conduction pathways (BB+VRPV, BB+FO or BB+CS)

The black lines are with BB and VRPV block, red lines are with BB and FO block, and blue lines are with BB and CS block. Red and blue lines are overlapped since their simulated results were very similar (Note: for interpretation of the references to color in this figure legend, the reader is referred to the web version of this article)

experiments (Waldo et al., 1971), indicating that a single pathway block could not make P wave morphology satisfy the typical diagnostic criteria of IAB. The results also showed that when the VRPV pathway was in a normal condition, the FO or CS pathway block has minor influence on the atrial activation sequence and P wave morphology. So the importance of the four conduction pathways follows as BB, VRPV, FO, and CS (i.e., the superior pathway was more important than the inferior pathway).

This study also simulated the effect of blocking two conduction pathways. When BB and VRPV were both blocked, the activation wave could only pass through inferior pathways. This results in the retrograde activation of LA in the caudo-cranial direction, leading to biphasic P waves in lead V_1 and the inferior

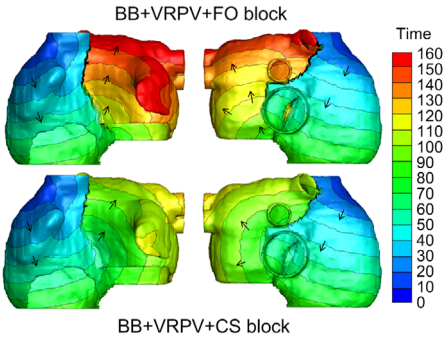

Fig. 7 Simulated activation sequences with the block of three conduction pathways

The arrows indicate the wave propagation direction. The color bar on the right-hand side indicates the propagation time with the unit in milliseconds (Note: for interpretation of the references to color in this figure legend, the reader is referred to the web version of this article)

Table 1 Summary of P wave duration and morphology with different combinations of conduction pathway blocks

Case	P wave duration (ms)	P wave morphology
Normal	103	Positive
BB block	113	Positive
VRPV block	104	Positive
FO block	105	Positive
CS block	103	Positive
BB+VRPV block	124	Biphasic
BB+FO block	114	Positive
BB+CS block	113	Positive
BB+VRPV+FO block	160	Biphasic
BB+VRPV+CS block	124	Biphasic

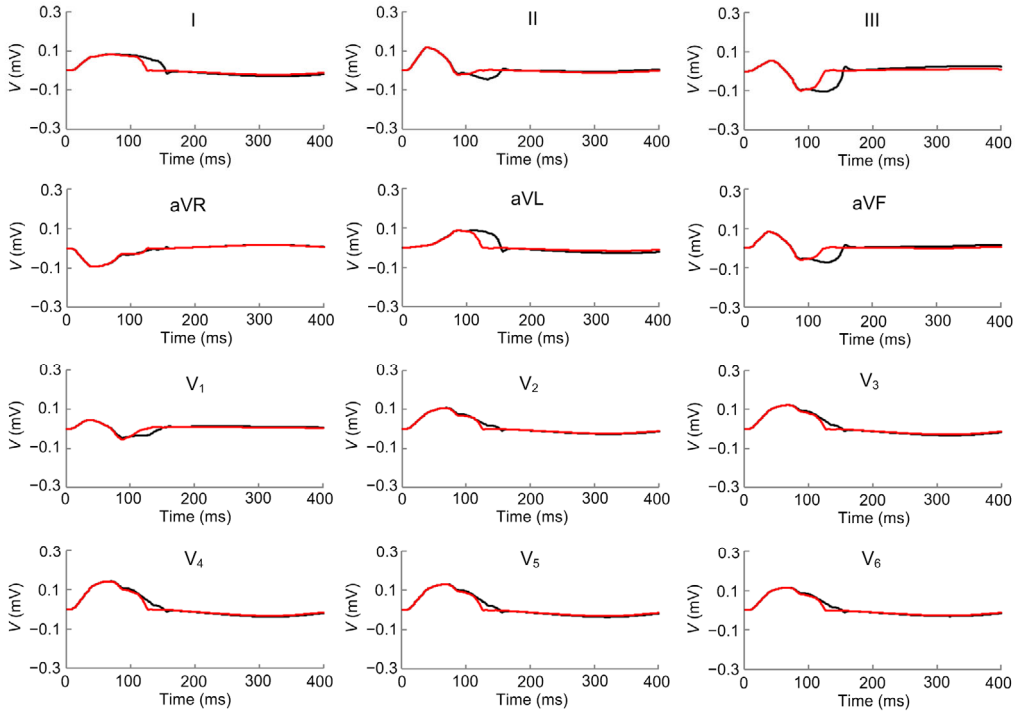

Fig. 8 Simulated P waves of 12-lead ECG with the block of three conduction pathways

The black lines are the BB, VRPV, and FO block; red lines are the BB, VRPV, and CS block (Note: for interpretation of the references to color in this figure legend, the reader is referred to the web version of this article)

leads (II, III, and aVF). The morphology and duration time all satisfied the diagnostic criteria of IAB. In the other two cases (BB and FO block, BB and CS block), due to the fact that the VRPV pathway was in a normal condition, the activation sequence of LA was still in a forward direction. Thus the P wave duration increased, but the morphology remained the same. These results indicated that retrograde activation of LA in the caudo-cranial direction was the substantial reason for P wave polarity change, so both BB and VRPV pathways play important roles in IAB.

The final finding from this study was that, when BB, VRPV, and FO were blocked, the retrograde activation of LA had the maximum propagation distance, leading to the longest P wave duration and significant biphasic P waves in lead V_1 and the inferior leads. When BB, VRPV, and CS were blocked, then because the FO pathway was superior to the CS pathway, the P wave duration was shorter and we also had biphasic P waves in lead V_1 and the inferior leads. This indicated that although a single inferior pathway plays a subordinate role in the inter-atrial conduction, the combination with other pathways could produce more severe IAB.

At present, clinical treatment of IAB has not yet reached a unified understanding. The study of biatrial pacing and RA appendage pacing on IAB showed that biatrial pacing could effectively reduce the concentrations of atrial natriuretic peptide (ANP) and markers of inflammation (high sensitivity C-reactive protein (hs-CRP), interleukin-6 (IL-6), and neopterin), indicating that biatrial pacing improved hemodynamic performance in patients with IAB and preserved atrioventricular conduction (Rubaj et al., 2013). Burri et al. (2011) also showed that biatrial pacing in comparison to pacing from interatrial septum or CS or RA appendage could result in favorable acute atrial hemodynamic and atrioventricular synchrony. The conclusions confirmed our simulation results, indicating that IAB is not caused by a single pathway block alone.

The studies of patients with SAN dysfunction and intra atrial conduction delay showed that low interatrial septum pacing could reduce P wave duration and prevent the development of persistent AF (Verlato et al., 2011; Lau et al., 2013). This is consistent with our simulation results of multichannel block, confirming that the role of inferior pathways cannot be ignored in IAB.

At present, biatrial pacing, atrial septum pacing, and Bachmann pacing all showed efficacy for the prevention of the occurrence of IAB. However, the sample size of each study is small and conclusions are varied. Therefore, these atrial pacing methods are currently not clinically recommended for the treatment of IAB. Our simulation results have a guiding role in explaining the mechanism of IAB and confirming the effect of pacing therapy and the placement of pacemakers. Moreover, according to the clinical diagnostic criteria of IAB, the lower limit of P wave duration of IAB has to be more than 120 ms, and our simulation showed that the P wave duration varied with different pathway blocks, indicating that P wave duration values may be used as an underlying tool to identify various combinations of pathway block.

It should be pointed out that there is a limitation in the present study. The model used in our simulation was a static heart model with electrophysiological properties. The mechanical functions of the heart have not been involved. Cardiac motion should be taken into consideration in future studies to improve simulation accuracy. In addition, our simulation results remain to be verified by means of experimental investigation. The block of the different electrical pathways in animals to study the ECG correlation would be the next step to confirm our theory.

5 Conclusions

In summary, this simulation study has demonstrated that at least the combinational block of BB and VRPV is required for the P wave duration and morphology to meet the typical diagnostic criteria of IAB. This provides a better understanding of the underlying mechanism of IAB and some guidelines for future pathophysiological and clinical studies of IAB.

Contributors

Yuan GAO performed the simulations and wrote the paper. Ying-lan GONG designed the simulations. Ling XIA put forward the importance of this purpose of the simulations. Dingchang ZHENG modified the paper. All authors read and approved the final manuscript. Therefore, all authors have full access to all the data in the study and take responsibility for the integrity and security of the data.

Compliance with ethics guidelines

Yuan GAO, Ying-lan GONG, Ling XIA, and Ding-chang ZHENG declare that they have no conflict of interest.

All procedures followed were in accordance with the ethical standards of the responsible committee on human experimentation (institutional and national) and with the Helsinki Declaration of 1975, as revised in 2008 (5). Informed consent was obtained from all patients for being included in the study.

References

Abe Y, Fukunami M, Yamada T, et al., 1997. Prediction of transition to chronic atrial fibrillation in patients with paroxysmal atrial fibrillation by signal-averaged electrocardiography: a prospective study. *Circulation*, 96(8): 2612-2616. https://doi.org/10.1161/01.CIR.96.8.2612

Ackerman MI, 1991. Viewpoint: the visible human project. *J Biocommun*, 18(2):14.

Alexander B, MacHaalany J, Lam B, et al., 2017. Comparison of the extent of coronary artery disease in patients with versus without interatrial block and implications for new-onset atrial fibrillation. *Am J Cardiol*, 119(8):1162-1165. https://doi.org/10.1016/j.amjcard.2016.12.032

Ariyarajah V, Spodick DH, 2006. The Bachmann Bundle and interatrial conduction. *Cardiol Rev*, 14(4):194-199. https://doi.org/10.1097/01.crd.0000195221.26979.2b

Ariyarajah V, Apiyasawat S, Najjar H, et al., 2007a. Frequency of interatrial block in patients with sinus rhythm hospitalized for stroke and comparison to those without interatrial block. *Am J Cardiol*, 99(1):49-52. https://doi.org/10.1016/j.amjcard.2006.07.060

Ariyarajah V, Kranis M, Apiyasawat S, et al., 2007b. Potential factors that affect electrocardiographic progression of interatrial block. *Ann Noninvasive Electrocardiol*, 12(1): 21-26. https://doi.org/10.1111/j.1542-474X.2007.00134.x

Bachmann G, 1916. The inter-auricular time interval. *Am J Physiol Legacy Content*, 41(3):309-320. https://doi.org/10.1152/ajplegacy.1916.41.3.309

Bayés de Luna A, Platonov P, Cosio FG, et al., 2012. Interatrial blocks. A separate entity from left atrial enlargement: a consensus report. *J Electrocardiol*, 45(5):445-451. https://doi.org/10.1016/j.jelectrocard.2012.06.029

Bayés de Luna A, Martínez-Sellés M, Bayés-Genís A, et al., 2017. Surface ECG interatrial block-guided treatment for stroke prevention: rationale for an attractive hypothesis. *BMC Cardiovasc Disord*, 17:211. https://doi.org/10.1186/s12872-017-0650-y

Burri H, Bennani I, Domenichini G, et al., 2011. Biatrial pacing improves atrial haemodynamics and atrioventricular timing compared with pacing from the right atrial appendage. *EP Europace*, 13(9):1262-1267. https://doi.org/10.1093/europace/eur099

Chhabra L, Devadoss R, Chaubey VK, et al., 2014. Interatrial block in the modern era. *Curr Cardiol Rev*, 10(3): 181-189. https://doi.org/10.2174/1573403X10666140514101748

Courtemanche M, Ramirez RJ, Nattel S, 1998. Ionic mechanisms underlying human atrial action potential properties: insights from a mathematical model. *Am J Physiol*, 275(1): H301-H321. https://doi.org/10.1152/ajpheart.1998.275.1.H301

Deng DD, Jiao PF, Ye XS, et al., 2012a. An image-based model of the whole human heart with detailed anatomical structure and fiber orientation. *Comput Math Methods Med*, 2012:891070. https://doi.org/10.1155/2012/891070

Deng DD, Gong YL, Shou GF, et al., 2012b. Simulation of biatrial conduction via different pathways during sinus rhythm with a detailed human atrial model. *J Zhejiang Univ-Sci B (Biomed & Biotechnol)*, 13(9):676-694. https://doi.org/10.1631/jzus.B1100339

Enriquez A, Sarrias A, Villuendas R, et al., 2015. New-onset atrial fibrillation after cavotricuspid isthmus ablation: identification of advanced interatrial block is key. *EP Europace*, 17(8):1289-1293. https://doi.org/10.1093/europace/euu379

Fernández-Fernández FJ, 2017. Atrial fibrillation: interatrial block may be an underdiagnosed and easily recognizable risk factor. *Mayo Clin Proc*, 92(4):681-682. https://doi.org/10.1016/j.mayocp.2017.01.022

Gao Y, Xia L, Gong YL, et al., 2018. Electrocardiogram (ECG) patterns of left anterior fascicular block and conduction impairment in ventricular myocardium: a whole-heart model-based simulation study. *J Zhejiang Univ-Sci B (Biomed & Biotechnol)*, 19(1):49-56. https://doi.org/10.1631/jzus.B1700029

Gialafos E, Psaltopoulou T, Papaioannou TG, et al., 2007. Prevalence of interatrial block in young healthy men <35 years of age. *Am J Cardiol*, 100(6):995-997. https://doi.org/10.1016/j.amjcard.2007.04.041

Gong YL, Gao Y, Lu ZH, et al., 2015. Preliminary simulation study of atrial fibrillation treatment procedure based on a detailed human atrial model. *J Clin Trial Cardiol*, 2(4): 1-9. https://doi.org/10.15226/2374-6882/2/4/00130

He JL, Tse G, Korantzopoulos P, et al., 2017. P-wave indices and risk of ischemic stroke: a systematic review and meta-analysis. *Stroke*, 48(8):2066-2072. https://doi.org/10.1161/STROKEAHA.117.017293

Kitkungvan D, Spodick DH, 2009. Interatrial block: is it time for more attention? *J Electrocardiol*, 42(6):687-692. https://doi.org/10.1016/j.jelectrocard.2009.07.016

Kligfield P, Gettes LS, Bailey JJ, et al., 2007. Recommendations for the standardization and interpretation of the electrocardiogram: Part I: the electrocardiogram and its technology: a scientific statement from the American Heart Association Electrocardiography and Arrhythmias Committee, Council on Clinical Cardiology; the American College of Cardiology Foundation; and the Heart Rhythm Society. *J Am Coll Cardiol*, 49(10):1109-1127.

https://doi.org/10.1016/j.jacc.2007.01.024

Lau CP, Tachapong N, Wang CC, et al., 2013. Prospective randomized study to assess the efficacy of site and rate of atrial pacing on long-term progression of atrial fibrillation in sick sinus syndrome: septal pacing for atrial fibrillation suppression evaluation (SAFE) study. *Circulation*, 128(7): 687-693. https://doi.org/10.1161/CIRCULATIONAHA.113.001644

Martínez-Sellés M, Massó-van Roessel A, Álvarez-García J, et al., 2016. Interatrial block and atrial arrhythmias in centenarians: prevalence, associations, and clinical implications. *Heart Rhythm*, 13(3):645-651. https://doi.org/10.1016/j.hrthm.2015.10.034

Martínez-Sellés M, Baranchuk A, Elosua R, et al., 2017. Rationale and design of the BAYES (Interatrial Block and Yearly Events) registry. *Clin Cardiol*, 40(4):196-199. https://doi.org/10.1002/clc.22647

Massó-van Roessel A, Escobar-Robledo LA, Dégano IR, et al., 2017. Analysis of the association between electrocardiographic P-wave characteristics and atrial fibrillation in the REGICOR study. *Rev Esp Cardiol (Engl Ed)*, 70(10): 841-847. https://doi.org/10.1016/j.rec.2017.02.019

O'Neal WT, Zhang ZM, Loehr LR, et al., 2016. Electrocardiographic advanced interatrial block and atrial fibrillation risk in the general population. *Am J Cardiol*, 117(11): 1755-1759. https://doi.org/10.1016/j.amjcard.2016.03.013

Rubaj A, Rucinski P, Kutarski A, et al., 2013. Cardiac hemodynamics and proinflammatory cytokines during biatrial and right atrial appendage pacing in patients with interatrial block. *J Interv Card Electrophysiol*, 37(2):147-154. https://doi.org/10.1007/s10840-013-9792-8

Shou GF, Xia L, Jiang MF, et al., 2007. Forward and inverse solutions of electrocardiography problem using an adaptive BEM method. Proc 4th Int Conf on Functional Imaging and Modeling of the Heart, p.290-299. https://doi.org/10.1007/978-3-540-72907-5_30

Spodick DH, Ariyarajah V, 2009. Interatrial block: the pandemic remains poorly perceived. *Pacing Clin Electrophysiol*, 32(5):667-672. https://doi.org/10.1111/j.1540-8159.2009.02343.x

Tapanainen JM, Jurkko RF, Holmqvist F, et al., 2009. Interatrial right-to-left conduction in patients with paroxysmal atrial fibrillation. *J Interv Card Electrophysiol*, 25(2): 117-122. https://doi.org/10.1007/s10840-008-9359-2

Tekkesin AI, Çinier G, Cakilli Y, et al., 2017. Interatrial block predicts atrial high rate episodes detected by cardiac implantable electronic devices. *J Electrocardiol*, 50(2):234-237. https://doi.org/10.1016/j.jelectrocard.2016.09.004

Tse G, Lai ETH, Yeo JM, et al., 2016. Electrophysiological mechanisms of Bayés syndrome: insights from clinical and mouse studies. *Front Physiol*, 7:188. https://doi.org/10.3389/fphys.2016.00188

Tse G, Wong CW, Gong MQ, et al., 2017. Predictive value of inter-atrial block for new onset or recurrent atrial fibrillation: a systematic review and meta-analysis. *Int J Cardiol*, 250:152-156. https://doi.org/10.1016/j.ijcard.2017.09.176

Verlato R, Botto GL, Massa R, et al., 2011. Efficacy of low interatrial septum and right atrial appendage pacing for prevention of permanent atrial fibrillation in patients with sinus node disease: results from the electrophysiology-guided pacing site selection (EPASS) study. *Circ Arrhythm Electrophysiol*, 4(6):844-850. https://doi.org/10.1161/CIRCEP.110.957126

Waldo AL, Bush HL Jr, Gelband H, et al., 1971. Effects on the canine P wave of discrete lesions in the specialized atrial tracts. *Circ Res*, 29(5):452-467. https://doi.org/10.1161/01.RES.29.5.452

Wu JT, Wang SL, Chu YJ, et al., 2017. $CHADS_2$ and CHA_2DS_2-VASc scores predict the risk of ischemic stroke outcome in patients with interatrial block without atrial fibrillation. *J Atheroscler Thromb*, 24(2):176-184. https://doi.org/10.5551/jat.34900

Xia L, Huo M, Wei Q, et al., 2006. Electrodynamic heart model construction and ECG simulation. *Methods Inf Med*, 45(5):564-573. https://doi.org/10.1055/s-0038-1634119

Zhang Y, Xia L, Gong YL, et al., 2007. Parallel solution in simulation of cardiac excitation anisotropic propagation. Proc 4th Int Conf on Functional Imaging and Modeling of the Heart, p.170-179. https://doi.org/10.1007/978-3-540-72907-5_18

中文概要

题　目：基于人体心房模型的房间阻滞仿真

目　的：探究不同心房间传导通道阻滞的组合对形成房间阻滞的影响及体表心电图变化，探究房间阻滞的产生机理。

创新点：通过仿真证明了单一 Bachmann 束阻滞并不能产生典型的房间阻滞 P 波时长和波形，并结合电兴奋传导时序，解释了房间阻滞的产生机理。

方　法：通过 64 位螺旋电子计算机断层扫描（CT）扫描人体心房，构建心房解剖模型。阻断不同的心房间传导通道，以单域方程仿真出心房电兴奋传导时序，采用边界元法计算各时刻人体体表电位，进而计算出 P 波波形。

结　论：要使 P 波时长和形态均满足临床诊断房间阻滞的条件，必须同时阻断 Bachmann 束和右肺静脉后部的穿间隔纤维（VRPV）通道，这为进一步了解房间阻滞的发病机制及未来临床研究提供了指导。

关键词：房间阻滞；心电图；仿真；心脏建模